UNIVERSITY OF TWENTE.

Master thesis
Systems and Control - Robotics & Mechatronics

The bird is the word

Port based Hamiltonian modelling of flapping wing aeroelasticity using vacuum chamber and wind tunnel measurements

Berend Antoine van der Grinten
s0193178
September 4, 2015

Committee
Prof.dr.ir. S. Stramigioli
ir. G.A. Folkertsma
N. Nijenhuis Bsc.

ROBOTICS
AND
MECHATRONICS

Preface

Dear reader,

Thank you for reading my master thesis' document. I will use this preface to explain explain something about the work behind the academic results. Furthermore I will thank the most valuable contributors.

Thanks to Stefano Stramigioli I got introduced to this project. I choose to work on it for a few reasons: 1) I preferred my assignment to be related to a commercial project, 2) I preferred a multidisciplinary assignment, 3) I preferred a real challenge, and last but not least because the Robird is simply awesome. In hindsight, I am even more convinced that I have made the correct choice. I don't know any other project to which I would have contributed with more enthusiasm and conviction.

Initially, the idea was to map the accuracy of different rigid body models of a flapping wing using wind tunnel measurements. This is truly multidisciplinary since it involves: aerodynamics, screw theory dynamics, optimization algorithms, stereo vision, detection algorithms and a practical setup to measure in a wind tunnel. During the first weeks I got the idea to expand the project to also measure the dynamics in a vacuum chamber. This made the practical experiments much more complicated. Furthermore, it involved more managing of people and institutions. However, theoretically it could improve the accuracy of the model so I was given to the opportunity to try to work it out.

I did manage to do both experiments and I think I proved that I could switch between academic theory, practical implementations and managing the stakeholders.

Some say that the master theses project should be designed to bring the theory of the master courses into practise. I think that was not the case with my project since I have learned so much more during this project:

- Aerodynamics in theory and in practise
- Using Screw theory in a model
- Material behaviour in low pressure
- Genetic algorithms
- Tracking and tracing
- Stereo vision
- Video manipulation
- Basic Arduino programming

- Milling and turning of aluminium
- And even soldering

Unfortunately there are still a lot off 'lose ends' now that I finish this project. Mostly because the tracking was so much more work. Furthermore, I was delayed during the preparation for the vacuum chamber experiments. Lastly, I think I could have improved the results if I could have started earlier to bring just parts of it together. For too long I was aiming to do everything, next time I will be earlier with my decisions to converge the project.

I should confess that the results of this project would not have been remotely possible without my supervisor Geert Folkertsma. He implemented the complete detection and tracking algorithms to get the 3D trajectories. This was necessary since the project had grown simply to much to tackle by one person in 40 weeks. I cannot stress enough how much I liked our collaboration and how important Geert has been for this project. Thank you Geert!

Secondly I would like to thank Clear Flight Solutions and specifically Nico Nijenhuis for adopting me in his company. Nico embraced the opportunity to measure inside the vacuum chamber and made it (together with RAM) financially possible. Furthermore, I liked the many conversations I had with Clear Flight Solutions regarding engineering challenges to improve the Robird. I worked with great pleasure at CFS. I am confident that they will succeed creating a commercial succes.

My time at the University of Twente has been wonderful, mostly due to the active student community. I have accepted an offer in Eindhoven in lithographic systems. I hope to expand my knowledge in optics and I will continue to work on multidisciplinary high tech systems. This master assignment has been an excellent preparation for that. To all who wonder if they can fly:

Just spread your wings!

Berend van der Grinten

The bird is the word

Port based Hamiltonian modelling of flapping wing aeroelasticity using vacuum chamber and wind tunnel measurements

Berend A. van der Grinten*, Gerrit A. Folkertsma*, Nico Nijenhuis†, Stefano Stramigioli*
bvanderg@gmail.com, g.a.folkertsma@ieee.org, n.nijenhuis@clearflightsolutions.com, s.stramigioli@ieee.org
*Robotics and Mechatronics group, CTIT institute, University of Twente
†Clear Flight Solutions, Enschede, The Netherlands

***Abstract*—An aeroelastic dynamic model of a flapping wing is essential for developing effective control algorithms for robotic birds. In this study we present a port based Hamiltonian multi-rigid-body approach to model the flapping wing of the Robird: a robotic bird of prey. Three models with a respectively 4, 11 and 24 bodies have been created. Some -difficult to estimate-structural and aerodynamic parameters of these models have been estimated with a genetic algorithm. Input for this genetic algorithm are (besides the models) 3D measurements of the Robird's wing in both a vacuum chamber and wind tunnel. The result is a dynamic model of a flapping which simulates the dynamics of the wing of the Robird. It is proven that the genetic algorithm method contributes to the accuracy of the model. However, the largest errors in the model are probably due to the assumptions and simplifications. Therefore it remains unproven that the genetic algorithm is the best method to create more accurate models.**

I. Introduction

A. Bird control with a robotic falcon is useful

In many places, birds are a nuisance (eating seeds at farms, spreading waste around landfills) or even a hazard: plane-bird collisions cost millions in damage and may lead to severe accidents [1]. Methods to drive birds away from these places, such as visual and acoustic devices, quickly lose their effectiveness due to habituation; even population reduction is not very effective [2]. Falconry offers long-lasting effectiveness, because fear of predators is inbred in pest birds, but falcons are expensive to train and they cannot fly all day long. Even worse: now the falcons themselves form a hazard to planes [3].

The company Clear Flight Solutions[1] has developed a flapping wing robotic bird modelled after a peregrine falcon, they call it: the *Robird*. The flapping wing motion creates both the trust and the lift, while steering is achieved using flaps at the tail. The Robird's appearance is remarkably similar to an actual peregrine falcon (see fig. 1). Even better, the flapping wing motion of the Robird resembles nature so well that other birds instinctively act as if they encounter an actual predator: they flee the scene. Therefore, the Robird can be used as a cheap, reliable and effective tool for bird control.

[1] www.clearflightsolutions.com

Fig. 1: The peregrine falcon (left) and its robotic sister (right) look alike.

B. A dynamic model of the Robird must be developed

However, there is a problem. Due to the flapping of the wings, the Robird is intrinsically unstable and only the most experienced pilots can fly it. If the Robird were easier to use, it would be a cheaper and better tool against nuisance birds. Ideally, an operator should be able to tell the Robird to fly to GPS-coordinates or even to chase after a flock of birds: the Robird should become more autonomous. For the efficient development of the control algorithms a dynamic model of the bird is a necessity. With that model, one can test the autonomous functions in a simulation environment and save time and funds compared with a trail and error approach. Furthermore, a dynamic model can be used to improve the design of the Robird. For instance, it gives insight into the structural forces inside the wing and insight in the necessary torque of the motor during a wing beat.

II. Method

A. Modelling using Bond Graphs has distinct advantages

The preferred accuracy of the control will be in the order of meters. For instance, it is not significant if the Robird is chasing a flock of birds at 30 or 31 meters. Therefore, there is some margin to trade off accuracy of the dynamic model. Furthermore, to develop control algorithms it is beneficial if the model is relatively fast. If simulation takes a significant amount of time, it would result in slower development of the Robird.

Accurate models for fluid structure interaction use numeric methods such as Computational Fluid Dynamics (CFD). One drawback of CFD is that it is computationally expensive: reported CPU times for a flexible flapping wing model are 1 day [4] and 5 days [5]. This would hinder the model as a tool to develop control algorithms. A second drawback is that CFD does not work well with control algorithms.

Mechanics, electronics and control can be easily combined into one dynamic model using a multi domain technique such as bond graphs. Furthermore, a bond graph model can be used to optimize the actuation in terms of power consumption. Therefore, it is chosen to trade off the aerodynamic accuracy of CFD with the usability and functionality of bond graphs.

B. Both aerodynamic and structural parameters are difficult to estimate

The flapping wing is modelled using a limited number of rigid bodies (see section III-D). Each body is mechanically connected with the surrounding bodies using a 6D damper and 6D spring (see sections III-A and III-C). Parameters of these spring-damper combinations are not easy to estimate since the wing is not homogeneous.[2] Therefore, the 6D stiffness and especially the damping coefficients are difficult to measure and/or estimate.

Depending on the state of the bodies they and aerodynamic parameters of each body, a resulting aerodynamic force is calculated for each body (see section III-E). If one knowes the lift distribution is unknown; it is therefore difficult to estimate these aerodynamic parameters.

C. Measured dynamics of the wing are used to estimate these parameters

Using a heuristic search it is possible to optimize the estimation of the parameters as mentioned above. A genetic algorithm (GA) has been used for this search (see section IV-A). Input for this genetic algorithm are the measured dynamics of the real wing. Then, for a set of parameters the *fitness* can be determined by calculating the difference between the simulated dynamics and the measured dynamics according to some metric. If the difference is very small, the simulation matches the measurements closely, therefore the parameters are (likely to be) estimated accurately. Thus: parameter estimation can be improved using measured dynamics of the wing.

D. Accuracy is further improved by separating the dynamics due to aerodynamic forces

The genetic algorithm optimization could convert to a local optimum. This is a significant threat since aerodynamic and structural forces counteract each other. For example: if the wing tip bends to much in the simulation compared to the measurements, it might be (among others) that 1) the aerodynamic force is to large or 2) the stiffness of the wing is to low.

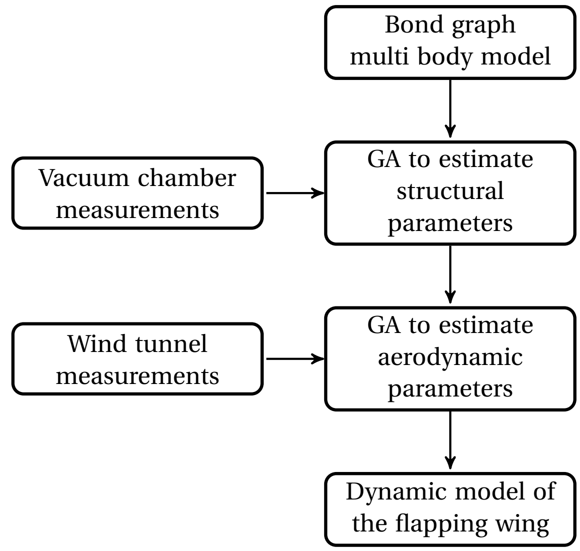

Fig. 2: The parameter estimation process is split in order to separately.

Using a vacuum chamber, it is possible to measure the dynamics of the wing with negligible aerodynamic influences. In simulation those measurements can be used to optimize the structural parameters of the wing: stiffness and damping. If, after that, the aerodynamics of the model are optimized using wind tunnel measurements, the aerodynamic optimisation is effectively decoupled from the rest of the model. Using both vacuum chamber and wind tunnel measurements can help preventing the convergence to local optima. Furthermore, using this method the error of the modelled aerodynamic forces can be separately evaluated.

E. Measuring the wing dynamics is relatively straightforward

The method for measuring the dynamics might be innovative for this application, but each individual step has been documented before in other articles. Therefore, it has been chosen to discuss the details of the measurement method only in an attachment (see appendix A). The main steps are:

- Markers are attached to the wing (see fig. 3)
- The wing is actuated with a constant flapping frequency using a setup based on [6]
- Two GoPro's[3] are used to create a stereo camera
- A stroboscope is used to film in 'slow motion'
- The markers are identified in each frame
- A 3D position of each marker is calculated
- A Kalman filter stitches each marker location to create trajectories

Thus, 3D trajectories of the markers of the wing are obtained in both the vacuum chamber and the wind tunnel,

[2]The main material of the wing of the Robird is EPP (Expanded polypropylene), the wing is strengthened with two carbon rods and one carbon strip. The rods can move in a slot created by a straw, the straw is glued with a rather heavy paste. The wing is covered with glue and a (quite sturdy) foil.

[3]GoPro Hero 4 Black edition, see www.gopro.com

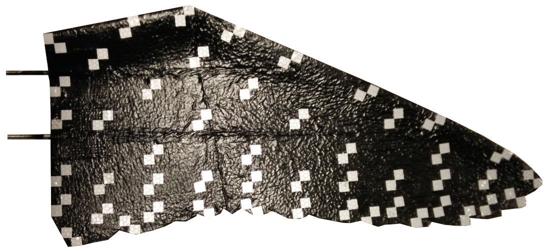

Fig. 3: The wing of the Robird with tracking markers.

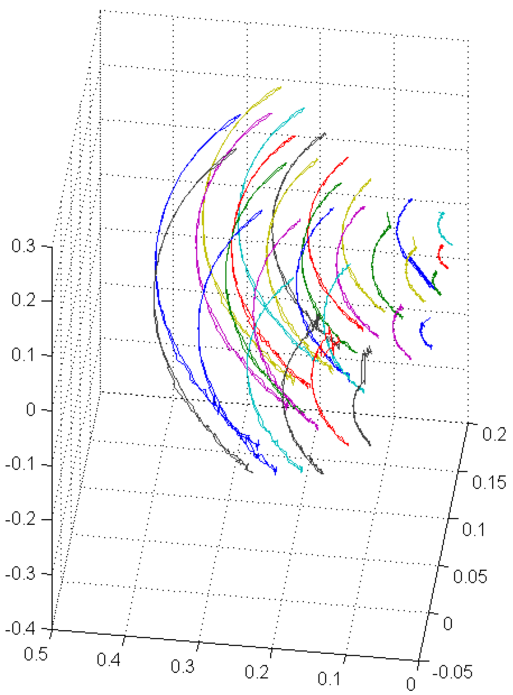

Fig. 4: Measured trajectories of the markers.

for different flapping frequencies and angles of attack of the wing. An example of these trajectories can be seen in fig. 4. This data is the input for the genetic algorithm as in fig. 2.

F. Broader applications of this work

As stated in section II-A this research uses a rigid body bond graph approach to model the dynamic aeroelasticity of the wing. The parameters are estimated using a genetic algorithm. Similar research includes: a bond graph model with *rigid* flapping wings [7], a *2D* bond graph model of flapping wings [8], a model of a robotic gull with *2 DOF in each wing* [9][10] and a 3D model of *flexible* wing [11]. To the knowledge of the authors, the method in this research is unique. Furthermore, this modelling method is not just applicable for modelling flapping wings, it provides a framework for modelling 3D dynamics of all flexible and rigid systems.

III. Rigid body model

As discussed in section II-A, a port based Hamiltonian method has been chosen. The ports in 3D dynamics are based on screw theory.

A. An introduction to screw theory for 3D dynamics

In screw theory, the port variables are a *twist* and a *wrench*. Both are 6-dimensional vectors constructed with a pairs of 3 dimensional vectors. A twist T contains the angular velocity vector ω and linear velocity vector v and a wrench W contains the torque vector τ and force vector F.

$$T_i^{O,j} = \begin{bmatrix} \omega \\ v \end{bmatrix}, \quad W_i^{O,j} = \begin{bmatrix} \tau \\ F \end{bmatrix}, \tag{1}$$

Each twist and wrench is a tensor, it describes a relation between two coordinate systems with respect to a coordinate system. For example, the twist in section III-A could describe the movement of body j with respect to body i as seen from coordinate system O.

A twist (or wrench) can be transformed to a different coordinate system using the Adjoint matrix of the homogeneous transformation matrix H.

$$T_i^{0,j} = \mathrm{Ad}_{H_B^0} T_i^{B,j} \tag{2}$$

$$(W_i^{B,j})^\top = \mathrm{Ad}_{H_B^0}^\top (W_i^{0,j})^\top \tag{3}$$

One should note that although the notation might look complicated, the equations itself are not. The total dynamics of the body can be described with respect to all coordinate systems with just one transformation. Therefore, a multi body systems with 2 bodies is just a bit less complicated than a multi body system with N bodies. For more details regarding this see “Geometry and screw theory for robotcis" by Stramigioli [12].

B. The model of one rigid body

The bond graph model of the body can be seen in fig. 5. The central *1-junction* represents the twist $T_p^{p,0}$, which is the relative motion of the centre of mass (COM) with respect to the part P in the inertial frame (O), expressed in the inertial frame (P). The MGY is a screw theory equivalent for the Euler Junction System, this method is described by Desscher[13]. In short, the MGY accounts for the fictional forces and moments to model the gyroscopic effects. The equivalent aerodynamic force that act on the body are calculated externally. Using an MTF, one can add points where connectors will be attached. Depending on the number of connectors, this structure will be duplicated.

C. The model of one 6D connector between two bodies

Each body is connected with the surrounding bodies using a connecting element which represents a screw theory equivalent of a spring-damper combination. The bond graph of this connector can be seen in fig. 6. The spatial linear damping effects are modelled using an element R_6

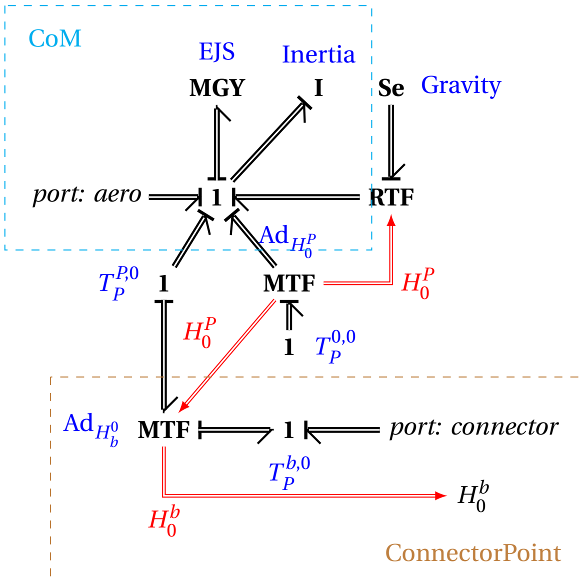

Fig. 5: The bond graph model of the body.

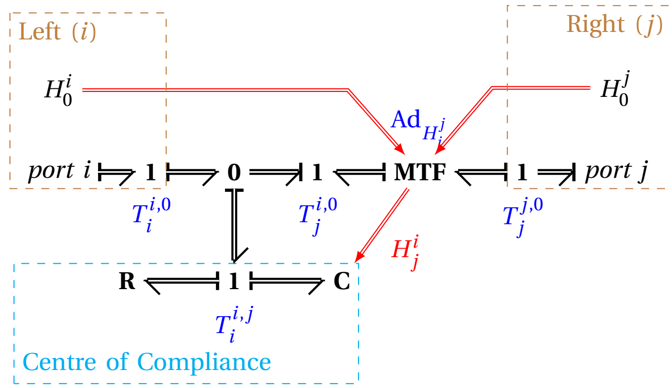

Fig. 6: The bond graph model of the connector.

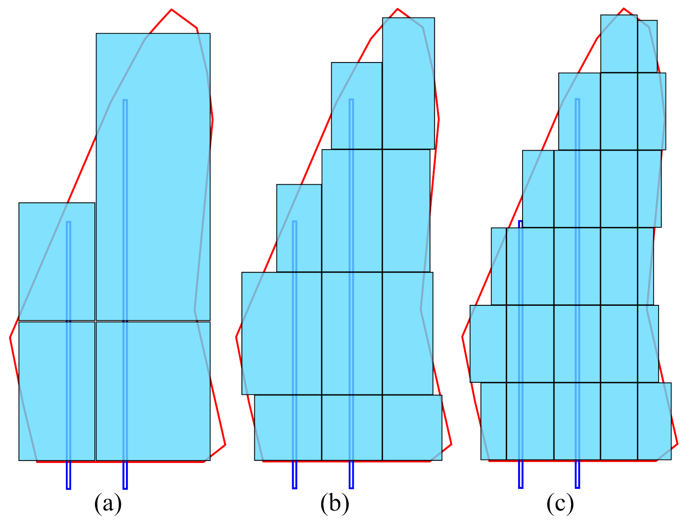

Fig. 7: Different designs of wing divisions.

which generates the dissipating wrench directly proportional to the relative twists of the connecting bodies.

$$(W_i^i)_{\text{diss}}^\top = R_6 T_i^{i,j} \tag{4}$$

The C_{6-D} accounts for the spatial compliance (a spring). The method is described by Stramigioli [12]. It describes an energy function based on the relative configuration H_i^j with a centre of compliance (the potential energy). Three 3×3 stiffness matrices K_o, K_t and K_c can be chosen, which correspond to the orientationial, translational and coupling stiffness parameters. Then, the co-stiffness parameters G_o, G_t and G_c can be calculated with:

$$G_\alpha = \frac{1}{2} tr(K_\alpha) I - K_\alpha \tag{5}$$

where $\alpha = o, t, c$ and tr is the trace operator (the sum of the diagonal elements). The wrench W_i^j (which consists of the moment m_i^i and force f_i^i) can then be calculated with:

$$m_i^i = \quad -2\mathrm{as}(G_o R_i^j) - \mathrm{as}(G_t R_j^i \tilde{p}_i^j \tilde{p}_i^j R_i^j) - 2\mathrm{as}(G_c \tilde{p}_i^j R_j^i) \tag{6}$$

$$\tilde{f}_i^i \quad = -R_j^i \mathrm{as}(G_t \tilde{p}_i^j) R_i^j - \mathrm{as}(G_t R_j^i \tilde{p}_i^j R_i^j) - 2\mathrm{as}(G_c R_j^i) \tag{7}$$

Where R_i^j and p_i^j are the rotation matrix and translation vector from the relative configuration H_i^j, *as* is an operator which takes the skew-symmetric part of a square matrix and the âĂŸtilde operatorâĂŹ is a cross product equivalent. For further information see Stramigioli [12].

D. Three different models have been created

Three different grids have been made with respectively 4, 11 and 24 bodies. It is expected that the design with 11 bodies will be sufficient to simulate most dynamics. 3, 11 and 24 bodies, which can be seen in fig. 7. For a design with more bodies (and thus more connectors), the computational time will increase. Therefore, these three designs have been chosen as a trade-off between the accuracy and the computational time. These designs will be used to investigate the coupling between the accuracy of the simulation and the number of bodies.

E. A straightforward aerodynamic model has been used

As can be seen in fig. 7, the wing is separated into bodies using a grid. A row of these bodies parallel to the body of the bird is called a strip. All the strips are parallel to each other and the bird, together the strips form the total wing. The aerodynamic forces (the lift and the drag) are calculated for each strip (the so-called modified strip theory[14]). The calculated lift of the total strip is distributed over the strips' bodies, which is illustrated in fig. 8. The total aerodynamic force (for a strip) is the sum of the lift F_L and the induced drag F_{ID}. Those components can be expressed as [9]:

$$F_L = \frac{1}{2}\rho v^2 S C_L(\alpha) \tag{8}$$

$$F_{ID} = \frac{1}{2}\rho v^2 S C_{ID}(\alpha) \tag{9}$$

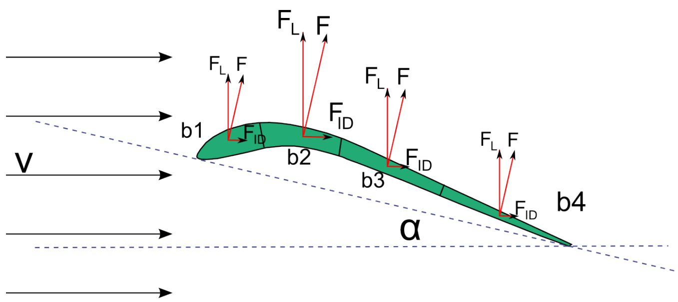

Fig. 8: The aerodynamic forces along the cord of a strip of the wing that is divided in four bodies.

Where ρ is the density of the air, v is the air flow relative to the wing (which is dependent on the flapping frequency), S is the area of the strip and C_L and C_{ID} are coefficients for Lift and Drag expressed as functions of the angle of attack α.

According to the estimation of Linton [15], the relation between the angle of attack and the coefficient of drag/lift is affine in the lower regions of the angle of attack (up to 15 deg). Therefore it is estimated that:

$$C_L(\alpha) = L_a\alpha + L_b \tag{10}$$

$$C_{ID}(\alpha) = ID_a\alpha + ID_b \tag{11}$$

Thus, the total aerodynamic force for each strip can be calculated. It still needs to be distributed over the bodies of the strip. This distribution is dependent of the angle of attack, as has been show by [16]. However, the total force is already dependent on the angle of attack, therefore (as a simplification) it is assumed that the distribution along the strip is constant during a wing beat.

$$F_L = L_1 F_L + L_2 F_L \dots L_N F_L \tag{12}$$

$$F_{ID} = ID_1 F_{ID} + ID_2 F_{ID} \dots ID_n F_{ID} \tag{13}$$

The sum of the coefficients L_i and ID_i both add up to one; these parameters can be estimated with the genetic algorithm and the available measurements. It should be stated that this aerodynamic model is very basic, the lift is purely based on the current angle of attack and (for instance) not on the previous angle of attack. Therefore, this method is not as accurate as a CFD based method as discussed in section II-A.

F. The actuation is velocity controlled

The wing in de Robird is actuated using two rods. The rear rod has a phase lag with respect to the front rod. This creates a changing angle of attack for the up and down-stroke of the wing; which contributes to the thrust. Since the motor inside the Robird is relatively strong, it is assumed that the actuation rods are velocity controlled. The actuation profile of the Robird is described by Vaseur [6].

IV. Parameter estimation using a genetic algorithm

A genetic algorithm (GA) is an optimisation algorithm that is based on the concepts of natural selection and natural genetics [17]. This effectively increases the likelihood that a global optimum is found instead of a local optimum. As introduced in section II-C, a GA is used to estimate (some) parameters of the flapping wing model. We will refer to such a parameter as a *gene*. Each model of the flapping wing with a certain *genome* will be referred to as an *individual*. Just as in natural selection, the genome varies between individuals; this variation determines the *fitness* of each individual. The fitter individuals are *selected* to create offspring. Offspring has some of the genomes inherited from their parents. Furthermore, mutations are present during reproduction. If one iterates over a large number of generations, the fitness of each population will be optimised. One can terminate the iteration if either the average fitness does not increase any more or if the fitness is already 'good' enough. This should translate to a flapping wing model whose parameters are adopted such that the fitness function is optimized. A flowchart that illustrates the process can be seen in fig. 9.
The total set of genes is called G. This set has two subsets: G_s and G_a for respectively the structural and the aerodynamic genes. Each parameter in G is bounded with an upper and lower bound. The GA will search within this range to find an optimum for each variable in G.

A. The genetic algorithm fitness function is based on the marker trajectories

After each individual model has been simulated using *20-sim*, the positions of the simulated tracking markers are exported to MATLAB. If there are N markers and one measures the data of a full wing beat (starting at t_s and ending at t_e), the dataset is represent as: $s_{[1:N],[t_s:t_e]}$. These are compared with the measured positions of the (real) tracking markers $m_{[1:N],[t_s:t_e]}$.
The fitness function has been chosen as the sum of the squared euclidean distances of each marker for each time step during one wing beat:

$$F = \sum_{t=t_s}^{t_e} \sum_{i=1}^{N} d^2\left(m_{i,t}, s_{i,t}\right) \tag{14}$$

One should notice that it is important that both the simulation data and the measured data are obtained during a wing beat where start-up effects are negligible and the flapping frequency is consistent. Furthermore, the data needs to be synchronised. Therefore, one should define a 'start' of a wing beat based on the position data. Since the wing is moving fast during a stroke, it will be sufficiently accurate to define the start of each wing beat when the front body corner crosses the horizontal position during an upstroke.

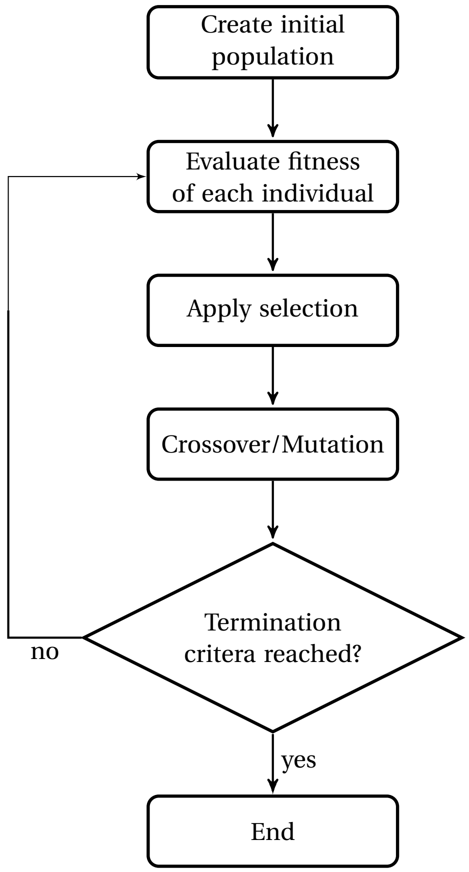

Fig. 9: Flowchart of a genetic algorithm.

B. The inertia and dimension parameters can be estimated without the GA

The dimensions of the wing of the Robird are very well known, therefore the dimensions of the different subdivisions of bodies (see fig. 7) are easy to estimate. Furthermore, the orientation of the bodies at rest can also be easily determined by measuring the aerofoil of the wing. Since the wing is non uniform (see footnote 2) the inertia of each body is a little bit more complex but it is still straightforward since the design of the wing is well known.

C. Parameter estimation for the connector

As stated in section III-C, the 6-dimensional damping map R and the three 3×3 stiffness matrices K_o, K_t and K_c have to be estimated for each connector. In a simplified view one can see the 6D spring-damper combination as 6 independent linear spring-damper combinations. This will greatly simplify the connectors since K_c will be zero and K_o and K_t will be diagonal matrices. As an example, we consider a connector which represents the connection between two foam bodies with a carbon rod (see footnote 2) along the y-direction:

$$K_o = \begin{bmatrix} E_f I_x + E_{rod} I_r & 0 & 0 \\ 0 & G_f I_y & 0 \\ 0 & 0 & E_f I_z + E_r I_r \end{bmatrix} \quad (15)$$

$$K_t = \begin{bmatrix} G_f A + G_r A_r & 0 & 0 \\ 0 & E_f A & 0 \\ 0 & 0 & G_f A + G_r A_r \end{bmatrix} \quad (16)$$

Where: A is the connecting surface area of the foam bodies, A_r is the surface area of the carbon rod (r), I_α is the second moment of area, E_f and G_f are the Young's and Shear modulus for the combination of the foam f of the wing with the coating; E_r and G_r are the Young's and Shear modulus for the carbon rod together with the glue and paste. Since the bodies connect (in this example) along the y-direction, longitudinal elongation along the y-direction depends on the Young's modulus and lateral translation along the x- and z-direction depends on the Shear Modulus. For the rotation, the opposite arguments holds.
The rotational and translational damping factor is also estimated to be linear with respectively the second moment of area and the area. Thus, a similar model for the stiffness can be used.

$$R = \left[D_E I_x; D_G I_y; D_E I_z; D_G A; D_E A; D_G A\right]^\top \quad (17)$$

Where D_E and D_G are unknown damping coefficients, they act as the damping equivalent of the Young's and Shear modulus. For simplification it is estimated that the damping in the carbon rod is negligible. Thus, it is approximated that the damping between two bodies of the wing is only dependent on the dimensions of the connecting surface area and two damping coefficients.

It should be stressed that both the stiffness and damping moduli are hard to estimate since they represent combinations of different materials and material interfaces. Therefore these moduli are estimated with the genetic algorithm. Combined, these are the structural genes:

$$G_s = \left[E_f; E_r; G_f; G_r; D_E; D_G\right] \quad (18)$$

D. Parameter estimation for the aerodynamics

Referring to the aerodynamic model discussed in section III-E, the lift and drag coefficients have an affine relation with the angle of attack (see sections III-E and III-E). Since the aerofoil shape is assumed to be the same for the entire wing, only 4 parameters are left to estimate the total lift and drag for each strip: L_a, L_b, ID_a and ID_b. Furthermore, the total lift and induced drag have to be distributed over the wing. For simplification it is assumed that this is distribution is constant during the wing beat. Please note that the total lift still varies during a stroke, only the lift distribution is assumed to be constant. This leads to the following set of genes as input for the GA:

$$G_a = [L_a; L_b; ID_a; ID_b; L_1; L_2; L_3; L_4; ID_1; ID_2; ID_3; ID_4] \quad (19)$$

Fig. 10: A screenshots of a simulations for each different model

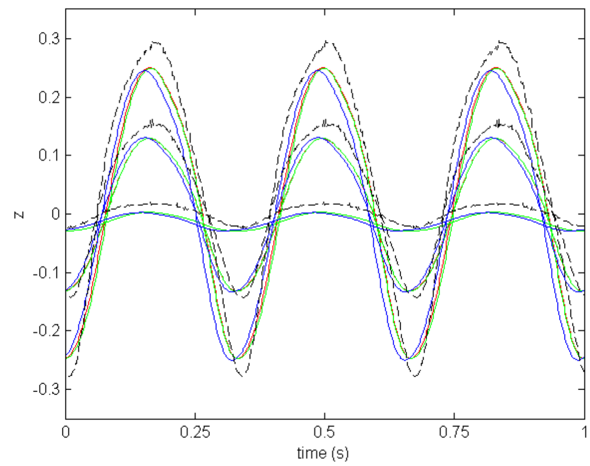

Fig. 11: The z-coordinate of some markers for the measured (dashed) and the three models of the simulated markers.

E. The other GA inputs

In the above sections the gene set and the fitness function have been defined. Less critical are the choices for the population size, a trade off between accuracy and computational effort [18]. A population size of 50 individuals has been chosen.
The boundaries for the genes have been chosen based on a (rough) estimation of the parameters. If the estimation is x, the lower and upper limit are respectively $0.2x$ and $5x$. Again, this is a trade-off between accuracy and computational effort.
The GA is set to terminate if the fitness of the best individual in the population has not changed for 10 successive populations. This is the stall parameter for the generations.

V. Results and error analysis

Screenshots of the different 3D animations can be seen in fig. 10. In a video, the dynamics seem to be natural and no sudden or unexpected behaviour is observed. Please note that only one wing is calculated; the second wing is a mirrored version for aesthetic purposes only.

When compared to the measurements, there seems to be a discrepancy: the z-coordinates for some markers during one wing stroke can be seen in fig. 11. In this figure, the three continuous red, blue and green lines represent a few markers for respectively the models with 4, 11 and 24 bodies. The black dashed lines are for the same measured markers. One can observe that the measured data is qualitatively similar for the 3 different models. However, there is a rather large difference between the simulated and the measured dynamics: it seems that the measured wing has a larger stroke. This can be further analysed in fig. 12. This figure is created using surface fits of the markers for a number of time instants during one upstroke in both the measured (blue) and simulated (green) data. The simulated data is created using the 24 body model. Ideally, the surface plots of both data sets would be overlapping each other. This seems to be the case in the horizontal position of the wing. However, for a smaller or larger angle of the wing, the measured data is quite different. Furthermore, there is a large difference near the base of the wing.

All three models have the problem that there is a large difference between the measured and simulated dynamics. Multiple factors could contribute to this:

- The calibration of the stereo camera set up is not accurate enough.
- The identification of the origin of the frame of the wing heavily influences the locations of the markers.
- The actuation profile in for the model is incorrect.
- The distance and/or frame between the rotational axis and the wing is incorrect in the model.

The last item is the most likely: if this is the case it would contribute to both the error in the base of the wing and to the error of the large stroke. Due to time constraints it is chosen to continue test to implement the genetic algorithm. Unfortunately, it is not expected that the genetic algorithm can help reducing these large errors since the base of the wing is velocity-controlled by the actuation model.

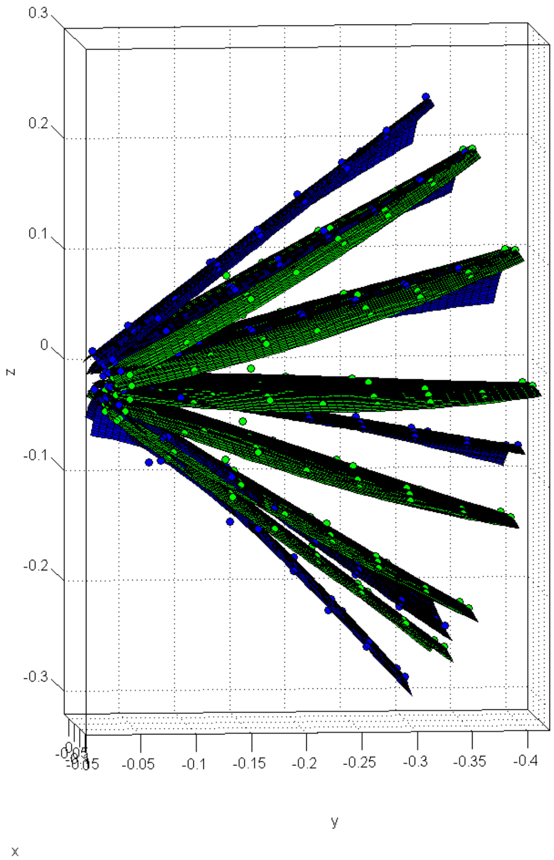

Fig. 12: The measured dynamics (blue) versus the simulated dynamics (green) in 3D.

A. The genetic algorithm results

The genetic algorithm function has been applied to improve the parameter estimation. However, due to the large errors which are explained above, it could not been proven that the genetic algorithm contributes much. The average fitness (as described by eq. (14)) is over 900 metres for each model. This calculates to an average Euclidean distance between the measured and simulated marker of about 2 centimetres. The result for the genetic algorithm optimization for the 24 bodies model can be seen in fig. 13. The computational time for this optimization was approximately 15 hours. This is mostly due to 20sim, which had to be restarted after each simulation in order to prevent crashes. The fitness value did decreases from an average of 970 to 956. Therefore, one can say that the roadmap to optimise a model using a genetic algorithm is correct. However, for this model the improvement is not significant.

The results as described above for the 24-bodies model is very similar to the results for the other two models. All fitnesses are in the range of 850 to 1000 metres after the genetic algorithm. The lack of significant differences between the three models is probably due to the systematic error in the actuation, which causes all other fluctuations to be negligible.

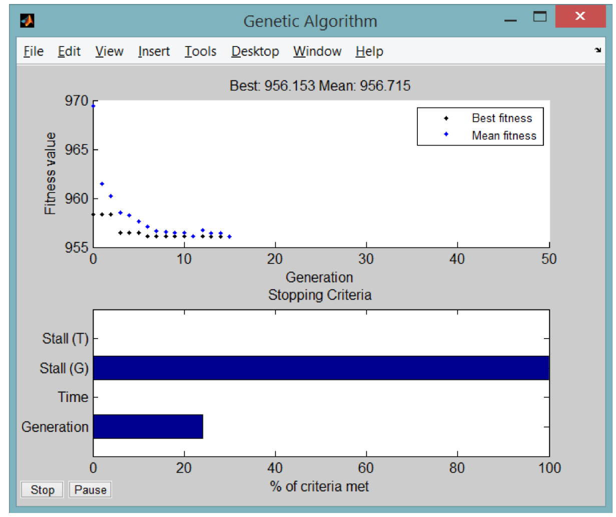

Fig. 13: A screenshot of the results of the genetic algorithm for the model with 24 bodies.

VI. Conclusion

Three different port-based Hamiltonian models of a flapping wing have been created. If one evaluates only the simulations, the dynamics seem to be natural and no sudden or unexpected behaviour is observed. The use of a genetic algorithm to estimate some parameters increased the accuracy of the model. However, the increase in accuracy due to the genetic algorithm is insufficient compared to the total error. Therefore, one can not conclude that the use of the genetic algorithm with the measurements is a unilateral success to optimise this particular model of a flapping wing.

Future research should conclude whether this method in practise is indeed more accurate. It is recommended that the models are validated more thoroughly and with different scenarios. An expert in video processing can contribute by extracting more accurate data from the videos.
The split in vacuum chamber and wind tunnel measurements is just in theory advantageous. Due to time limitations, the potential gained accuracy has not been validated. However, this split cannot have a negative influence. Further research is necessary to reflect on the necessity of this method. Luckily, the data has already been collected—it is just not yet implemented thoroughly into the models.
The three different models have respectively 4, 11 and 24 bodies. Due to their inaccuracy, these models are currently not suited for quantitative simulations. However, the model with 4 bodies is easy to understand and can be used to calculate the magnitude and direction of forces applied by the wing on the body of the robotic bird. The model with 24 bodies is useful for qualitative information about the structural forces inside parts of the wing. It may be used to calculate influences of density, structure, and weight of the wing.

It is not known whether any of these models can be used to fly a simulated bird in a 3D simulation—due to time constrictions that has not been evaluated. Since the aerodynamic model in this research is very simple, it is expected that more work is necessary on the aerodynamics before one can achieve such a complete model of a flying bird. However, future research should expand on this design method and these models since the theoretical benefits of this method are, although unproven, in principle still valid.

ACKNOWLEDGEMENTS

The authors would like to thank ESTEC—the European Space Agency—for their help measuring the wing dynamics in a vacuum chamber. Also, the authors would like to thank Clear Flight Solutions for their expertise and help regarding the Robird.

REFERENCES

[1] I. Maragakis, "Bird population trends and their impact on aviation safety 1999-2008," *Safety Analysis and Research Department, European Aviation Safety Agency*, 2009.

[2] M. Bomford and R. Sinclair, "Australian research on bird pests: impact, management and future directions," *Emu*, vol. 102, pp. 29–45, 2002. [Online]. Available: http://dx.doi.org/10.1071/MU01028

[3] P. Matyjasiak, "Methods of bird control at airports," *Theoretical and applied aspects of modern ecology. J. Uchmanski (ed.), Cardinal Stefan Wyszynski University Press, Warsaw*, pp. 171–203, 2008.

[4] K. Nakahashi, T. Fujita, and Y. Ito, "From one-month cfd to one-day cfd - efforts for reducing time and cost of cfd," in *New Developments in Computational Fluid Dynamics*, ser. Notes on Numerical Fluid Mechanics and Multidisciplinary Design (NNFM), K. Fujii, K. Nakahashi, S. Obayashi, and S. Komurasaki, Eds. Springer Berlin Heidelberg, 2005, vol. 90, pp. 68–80. [Online]. Available: http://dx.doi.org/10.1007/3-540-31261-7_7

[5] M. A. Jones, "Cfd analysis and design optimization of flapping wing flows," Ph.D. dissertation, 2013, aAI3609576.

[6] C. S. E. Vaseur, "Robird wind tunnel test setup design," MSc report 020RaM2014, University of Twente, Nov. 2014.

[7] D. Samuel, G. Sebastien, B. Alexandre, C. Eric, and C. Daniel, "Bond graph model of a flapping wing micro-air vehicle," in *Mechatronic and Embedded Systems and Applications (MESA), 2014 IEEE/ASME 10th International Conference on.* IEEE, 2014, pp. 1–6.

[8] Z. Jahanbin, A. Selk Ghafari, A. Ebrahimi, and A. Meghdari, "Multi-body simulation of a flapping-wing robot using an efficient dynamical model," *Journal of the Brazilian Society of Mechanical Sciences and Engineering*, pp. 1–17, 2015. [Online]. Available: http://dx.doi.org/10.1007/s40430-015-0350-4

[9] M. S. Couceiro, C. M. Figueiredo, N. F. Ferreira, and J. T. Machado, "Simulation of a robotic bird," *Fractional differentiation and its applications, Ankara*, 2008.

[10] ——, "The dynamic modeling of a bird robot," in *9th Conference on Autonomous Robot Systems and Competitions, Robotica*, 2009.

[11] A. T. Pfeiffer, J.-S. Lee, J.-H. Han, and H. Baier, "Ornithopter flight simulation based on flexible multi-body dynamics," *Journal of Bionic Engineering*, vol. 7, no. 1, pp. 102 – 111, 2010. [Online]. Available: http://www.sciencedirect.com/science/article/pii/S167265290960189X

[12] S. Stramigioli and H. Bruyninckx, "Geometry and screw theory for robotics," *Tutorial during ICRA*, vol. 2001, 2001.

[13] D. Dresscher, Y. Brodskiy, P. Breedveld, J. Broenink, and S. Stramigioli, "Modeling of the youbot in a serial link structure using twists and wrenches in a bond graph," in *Proceedings of SIMPAR 2010 Workshops.* Germany: SIMPAR, November 2010, pp. 385–400. [Online]. Available: http://doc.utwente.nl/76356/

[14] D.-K. Kim, J.-S. Lee, J.-Y. Lee, and J.-H. Han, "An aeroelastic analysis of a flexible flapping wing using modified strip theory," in *The 15th International Symposium on: Smart Structures and Materials & Nondestructive Evaluation and Health Monitoring.* International Society for Optics and Photonics, 2008, pp. 69 281O–69 281O.

[15] J. O. Linton, "The physics of flight: Ii. flapping wings," *Physics Education*, vol. 42, no. 4, p. 358, 2007. [Online]. Available: http://stacks.iop.org/0031-9120/42/i=4/a=004

[16] P. E. Illman, *The pilot's handbook of aeronautical knowledge.* TAB books, 1995.

[17] J. H. Holland, *Adaptation in natural and artificial systems: an introductory analysis with applications to biology, control, and artificial intelligence.* MIT press, 1992.

[18] S. G. B. RYLANDER, "Optimal population size and the genetic algorithm," *Population*, vol. 100, no. 400, p. 900, 2002.

Appendix A

Measuring the dynamics of a flapping wing inside a wind tunnel and vacuum chamber

I. Introduction

Interactions between inertial, elastic, and aerodynamic forces that occur when an elastic body is exposed to a fluid flow are called the *aeroelastic* effects. For flapping wing flight these effects are essential to create thrust [1]. Aeroelastic effects are difficult to model and to validate. It is quite likely that an error in the inertial part of the model can be misidentified as an error in the aerodynamic part of the model, or vice versa. For instance, if the tip of a flapping wing model lags behind during an upstroke with respect to measured dynamics, it could be (among others) that the calculated lift is too small—or that the moment of inertia of the tip is too large. Therefore, to increase the accuracy of the model, one would prefer to separately validate the aerodynamic effects, and the inertial and elastic effects. This requires that the dynamics of the wing are measured both in a vacuum chamber and in a wind tunnel.

This research discusses the method, design choices and results of measuring the dynamics of the flapping wing of the Robird[1] in both a vacuum chamber and a wind tunnel. Although the application is the measurement of a flapping wing, this method could be used for a wide range of applications where tracking of an object is necessary.

II. Hardware

Two functions can be identified: actuation and measurement. For versatility they are designed such that they can be used in both the vacuum chamber[2] and the wind tunnel[3] There are some specific requirements in both environments:

The dimensions
: The vacuum chamber (see fig. 1) is a cylinder with a diameter of 0.7 m and a depth of 1.2 m. Both the wing and measurement setup should fit inside.
: The wind tunnel has an exit of about 0.7 by 1.0 m (see fig. 1) and only the flapping wing should be interfering with the flow. Therefore the measurement and actuation equipment should be away of the flow exit.

Contamination due to outgassing
: The low pressure inside the chamber could release gasses from the setup. This could contaminate the vacuum chamber. The use of soft materials such as rubbers, most glues and tape is prohibited.

Overheating
: Due the low pressure inside the vacuum chamber, heat convection will be near to zero. This could lead to overheating of the equipment.

[1] A robotic bird of prey created by Clear Flight Solutions

[2] A vacuum chamber from ESA has been used. It is located at the European Space Research and Technology Centre (ESTEC) in Noordwijk, the Netherlands.

[3] The wind tunnel from the Fluid Dynamics Group (University of Twente) has been used.

Fig. 1. The vacuum chamber (left) and the wind tunnel (right).

A. Actuation

The wing is actuated using two driving rods. The rear driving rod has a phase lag relative to the front driving rod. This phase lag is expected to be very important for the generated thrust of the wing. One of the goals of this setup is to evaluate the relation between the phase lag and the dynamics. Therefore, two motors and controllers are necessary to control the required phase lag. Each motor is attached to a four bar linkage system that creates a flapping motion.

The actuation setup is a mechanically modified version of Vaseur [2]. One of the changes is that all parts are in aluminium for improved robustness and heat dissipation. Furthermore, the motors have large mounts to increase the surface area of the connection to improve conduction. The setup is assembled with a heat conducting vacuum grease. The motors and the four bar linkage system are mounted on an aluminium ground plate which slides both into the vacuum chamber and in the wind tunnel. The system is schematically shown in fig. 2 and a picture can be seen in fig. 3.

B. Measurement system

In order to measure the dynamics, a stereo camera has recorded the flapping motion of the wing. Tracking markers

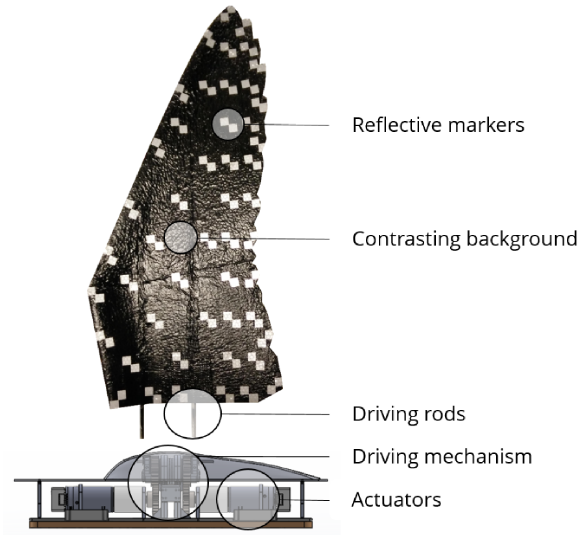

Fig. 2. A schematic view of the actuation setup with some name tags.

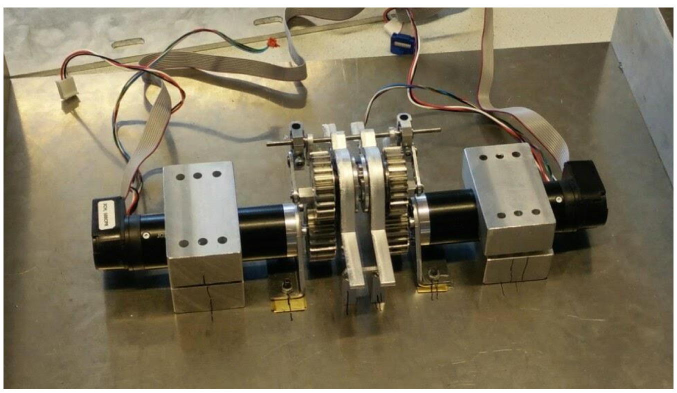

Fig. 3. The actuation system. The driving rods are mounted in the small cylinders.

have been applied on the wing, which can be seen in fig. 2. With the stereo camera one can deduce the 3D locations of each marker during each frame. If one stitches these 3D locations together they form 3D trajectories of the tracking markers; thus, identifying the dynamics of the wing.

C. Camera selection is difficult

The wing is flapping with a frequency of up to 4 Hz. Since the length of the wing is about 50 cm, the wing tip will be travelling up to $15\,\mathrm{m\,s^{-1}}$. Therefore (ideally) one would use high speed cameras to reduce motion blur and accurately record the fast moving markers on the wing. However, since the vacuum chamber does not have a large window, the cameras operate in a low pressure environment. There is a significant risk that released gasses from the rubbers and/or glues in de large cameras will contaminate the vacuum chamber. A second risk is that the low pressure environment destroys the expensive high speed camera: it might overheat or explode. Batteries must also be be protected from the low pressure. Thus, large complex and expensive cameras cannot be used, and it is best if the camera's power is outside vacuum chamber.

Not much information has been found regarding experiences to operate cameras in a low pressure environment. A couple of (non-academic) tests has indicated that GoPro cameras can operate in a partial vacuum [3]. It should be noted that building a protective case is relatively hard, mainly because it is much more difficult to keep pressure in than to keep pressure out. The conclusion is that the GoPro cameras are the most likely to survive. However, these are not high speed (up to 60 fps at 1080p). Simple test showed that motion blur during to the fast moving wing was quite significant. This would reduce the accuracy of the marker tracking.

D. A stroboscope helps to reduce motion blur

It is assumed that the flapping wing motion is periodic. Thus, after a number of wing beats—after start-up effects have disappeared—all next wingbeats will be indistinguishable from each other. Therefore one can use a stroboscope to create a slow-motion effect. The strobe frequency should be a little faster than the flapping frequency: then, if the ambient light is low and the strobe frequency is lower than the amount of frames per second, one could record each individual flash of the stroboscope. The use of a stroboscope has distinct advantages:

- The motion blur is not determined by the camera's exposure time, but by the length of one flash.
- The video speed is not determined by the camera but by the stroboscope. For example: if the flapping frequency is 3 Hz and the strobe frequency is 3.1 Hz, the camera effectively records 30 frames per wing beat.

Using a stroboscope can overcome the disadvantages of the GoPros. Furthermore, the stroboscope can be used to synchronise both GoPros: when the GoPros start recording (in a dark room), all frames will be black until the first flash of the stroboscope.

As stated above, each flash will be as short as possible to increase accuracy. The drawback is that a shorter flash may not be bright enough to illuminate the scene. This will increase the noise each frame and makes it harder to track the markers. Therefore, the wing has been painted black and the markers have been created using reflective tape. If the stroboscope is positioned near the camera, the flash will be reflected from each marker to the camera's sensor. The markers will be clearly visible and stand out to their environment (see fig. 2).

The stroboscope has been built using high-power LEDs, with an Arduino to control the flashing frequency. The LEDs have mounted around both cameras. The cameras are mounted in an aluminium frame to improve heat dissipation. The aluminium frames with the cameras are mounted on a ground plate that can slide in the vacuum chamber. The total measurement setup can be seen in fig. 4.

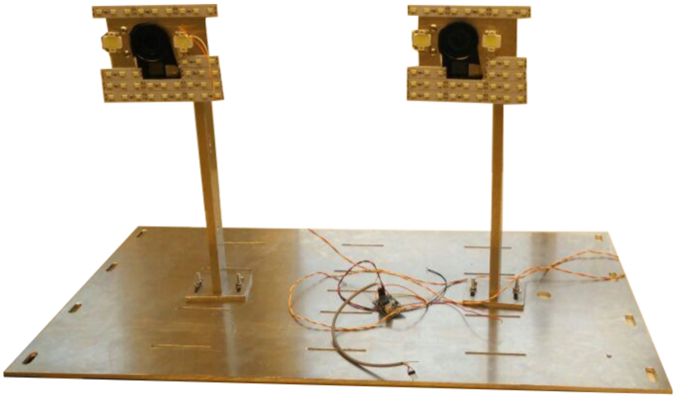

Fig. 4. The measurement setup with the two GoPros and the LEDs.

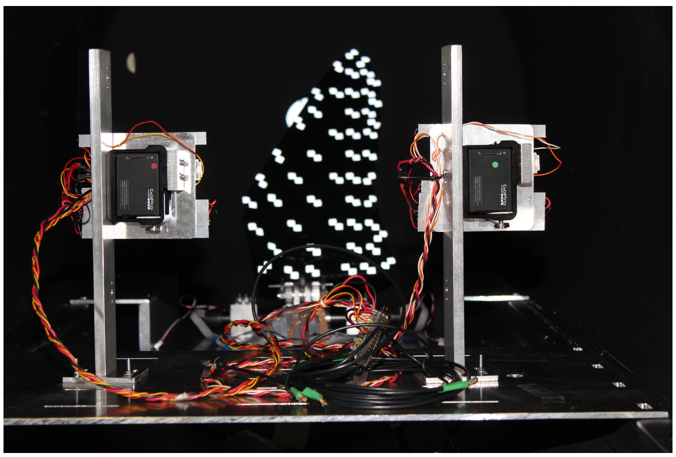

Fig. 5. The setup in the vacuum chamber.

E. Regarding the markers

The markers are created using 2 squares of reflective tape that are placed to form a 2×2 chequerboard. This shape has more features compared to a single dot with the same diameter as the width of the chequerboard. Since it has more features, the chequerboard marker is theoretically more accurate to detect. The positioning on the wing has been chosen such that the average marker density increases when the stiffness of the wing decreases. A lower stiffness will result in more flexing and thus more motion; therefore it makes sense to increase the marker density over wing towards the tip and towards the rear of the cord. There are a total of 49 markers, which is chosen as a a trade off between improved accuracy, and computational effort.

III. Testing

The total setup in the vacuum chamber can be seen in fig. 5. In order to gain understanding in the influence of aerodynamics it is opted to repeat all experiments at 1000 mbar, 100 mbar and at 10 mbar. In order to get more insight into the effect of the phase lag (as described in section II-A), all experiments have been repeated using 0°, 3° and 7° phase difference between the actuation rods.

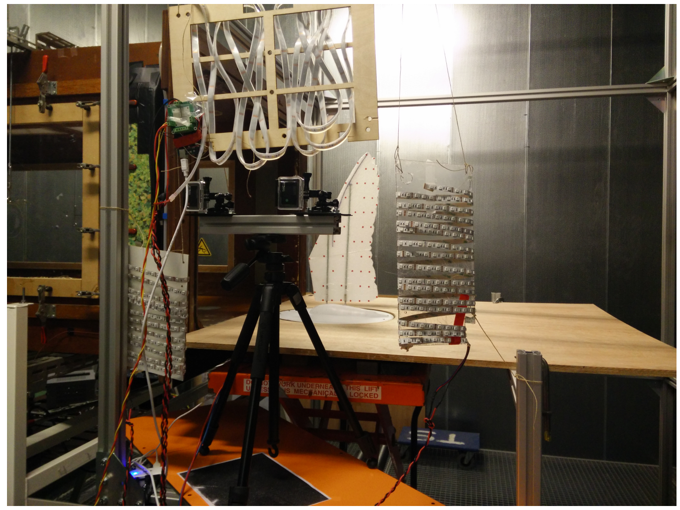

Fig. 6. The setup in the wind tunnel.

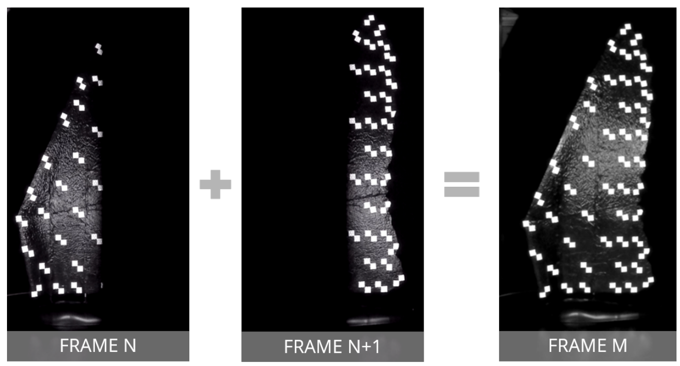

Fig. 7. Due to the rolling shutter of the GoPro consecutive frames must be combined to find all illuminated pixels from the strobe.

Lastly, all experiments have been repeated with flapping frequencies of 2 Hz, 3 Hz and 4 Hz.

For the experiments in the wind tunnel, the same sweep has been created regarding the phase lag and the flapping frequencies. Furthermore, all experiments have been repeated with five different wind speeds between $1\,\mathrm{m\,s^{-1}}$ and $11\,\mathrm{m\,s^{-1}}$. The total wind tunnel setup (with an older version of the wing) is shown in fig. 6.

IV. Data extraction from the videos

A. Video manipulation

The GoPros use a rolling shutter, which implies that each row of pixels on the sensor is read after the previous row of pixels has been read. Since the GoPros are not synchronised with the stroboscope, one can't time the stroboscope to flash just before the upper row of pixels will be evaluated. Therefore, the illuminated pixels from one flash of the stroboscope will be distributed over 2 consecutive partly-illuminated frames (this effect is shown in **??**). After that second frame, the next couple of frames will be black until the next flash illuminates 2 consecutive frames. One can

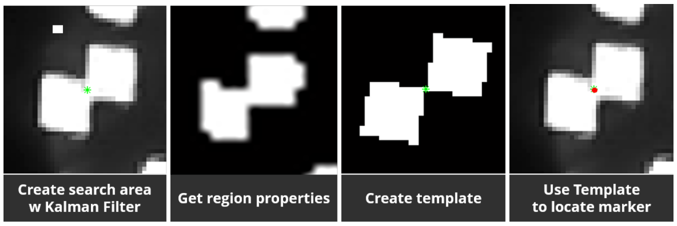

Fig. 8. The marker location process

thus easily detect if the a recorded frame has relevant data by thresholding the maximum value of each frame.

In order to gather all the data, each pair of consecutive illuminated frames is combined into one frame. Note that although the consecutive frames have a different timestamp, this is an effect of the rolling shutter: both frames belong to one flash and thus one time instant. The illuminated combined frames are stitched together to create a slow-motion video of the flapping wing.

B. Marker detection and tracking

The marker locations and orientations have been mapped and labelled for the wing at rest. These 3D locations are obtained by selecting the markers by hand and combining this data with the stereo camera calibration.[4] Because the marker is very bright compared to everything else in the frame, the markers can easily be extracted using a threshold on the brightness. The orientation of each marker can then obtained using the function `regionprops`.

With these known locations and projective geometry, a model has been made to predict the 3D location and the size of each marker based on the angle of the wing. Furthermore, this model can predict the skew of each marker in the 2D frames that are recorded by both cameras. To get a grasp of the model: it quantizes the prediction that if the wing turns away from the camera, the markers will shrink and the expected location will go down. Also, this will have a larger effect on the upper markers compared to the lower markers since the arm of the upper markers is longer.

Using this initial prediction regarding size and skew, a template of the marker is made (see the example at fig. 8). This template is fitted in an area around the predicted location using the function `normxcorr2`. This area is referred to as the search area (see fig. 8). The best fit of the template in the search area is most probably the location of the marker. This process is repeated until each marker location is detected. An example of a frame where all the markers succesfully are located can be seen in fig. 9.

C. Kalman filtering for tracking

When for a couple of frames the markers have been manually predicted and automatically detected with the method described above, 3D trajectories should be calculated. Furthermore, the prediction step should become automatic. The previous described prediction model assumes a rigid wing. Unfortunately this prediction is not accurate enough when the wing flexes during a wing beat. This creates problems keeping track which marker is labelled as such. Therefore, it is opted to predict purely based on the previous detections using a Kalman filter. The main steps are:

- Use the predicted size and skew to create a template of the marker
- Use the template and the predicted location to detect the marker
- Update the Kalman filter to combine the prediction and the detection
- Predict the next location of the marker
- Repeat all the above for each marker
- Repeat all the above for each frame

This creates 3D trajectories for each marker. It should be noticed that the prediction in the Kalman is just a simple constant acceleration model. This has been chosen for simplicity.

[4]Camera calibration has been performed using a chequerboard and standard MATLAB code to identify the the stereo camera parameters

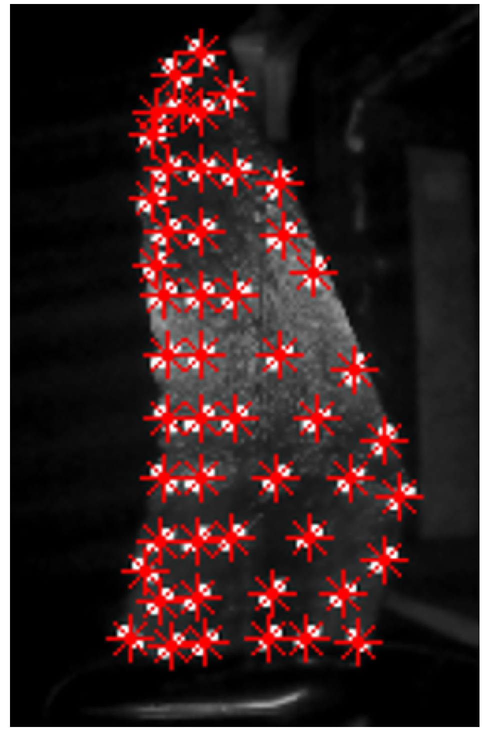

Fig. 9. All markers on the wing are located

V. Results

One of the trajectories can be seen in fig. 10. There are still some mistakes in the regions where the markers are more densely packed. From the 49 markers there are about 40 that have been tracked (partially) correctly. In fig. 11 the graph shows all the z-coordinate trajectories of the markers

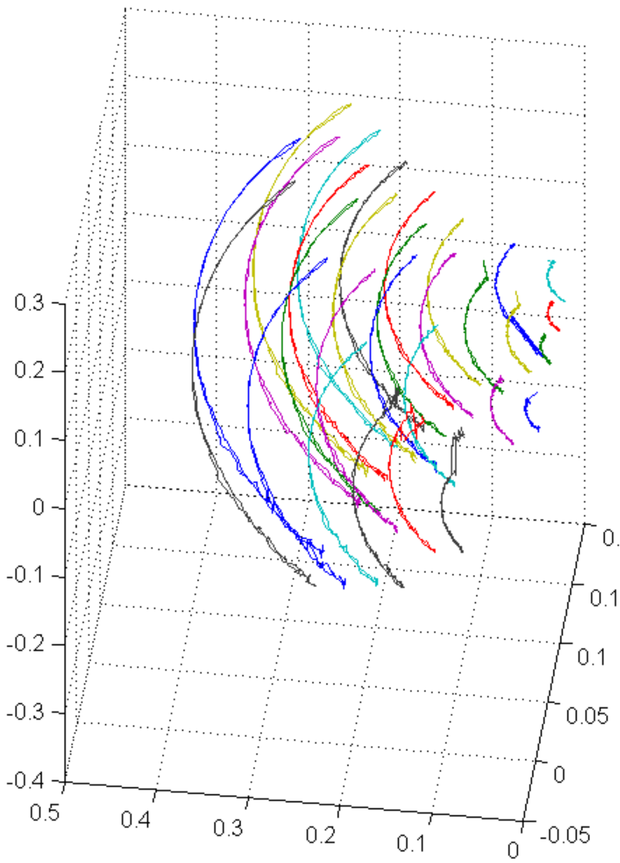

Fig. 10. 40 out of 49 markers can be tracked and visualised.

which are tracked in both the wind tunnel and the vacuum chamber flapping at 3Hz. There is a large difference. The wind tunnel wing has a distinct smaller stroke. Furthermore, the wind tunnel movement is much faster in the horizontal position. Both of this might be purely the effect of the air which dampens the movement of the wing. However, in the 3D simulation the movement of the vacuum chamber compared to the wind tunnel is quite interesting. It seems that there is a higher order of movement in the vacuum chamber data.

VI. Conclusion

The markers form a trajectory which is as expected. However, one can clearly see that there is still significant noise in the data. This is partly due to the parameters in the Kalman filter: it is a trade-off solution between smooth data and actual measured data. If the data had been smoothed more aggressively, it is likely that the measured flex of the wing will also be reduced, thus removing actual information. Furthermore, the noise appears to be quite random. In the genetic algorithm, white or high-frequent

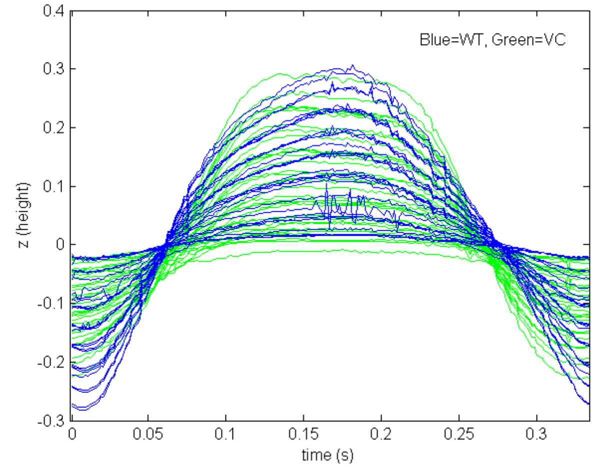

Fig. 11. z-coordinates of the markers for both the wind tunnel (WT) and the vacuum chamber (VC).

noise will be filtered anyhow since there are only static parameters tuned. Therefore, this result is regarded to be acceptable for the application it was built for. When the experiments will be repeated it could mainly be improved by increasing the number of frames per wing beat and averaging over these frames.

There are interesting differences between the trajectories in the wind tunnel and the vacuum chamber. It is definitely worth to further investigate the causes of these differences, these might give new insights in the forces on the wing.

References

[1] W. Shyy, H. Aono, S. Chimakurthi, P. Trizila, C.-K. Kang, C. Cesnik, and H. Liu, "Recent progress in flapping wing aerodynamics and aeroelasticity," *Progress in Aerospace Sciences*, vol. 46, no. 7, pp. 284 – 327, 2010. [Online]. Available: http://www.sciencedirect.com/science/article/pii/S0376042110000023

[2] C. S. E. Vaseur, "Robird wind tunnel test setup design," MSc report 020RaM2014, University of Twente, Nov. 2014.

[3] U. author. A small vacuum chamber test facility. [Online]. Available: http://www.citizensinspace.org/2014/02/a-small-vacuum-chamber-test-facility/